2011

Characterization of functional and structural deficits in a canine model of compressive optic neuropathy using optical coherence tomography and pattern electroretinography

Richard Nzoyem Nzokwe
Iowa State University

Characterization of functional and structural deficits in a canine model of compressive optic neuropathy using optical coherence tomography and pattern electroretinography

by

Richard Nzoyem Nzokwe

A thesis submitted to the graduate faculty

in partial fulfillment of the requirements for the degree of

MASTER OF SCIENCE

Major: Biomedical Sciences (Cell Biology)

Program of Study Committee:

Sinisa D. Grozdanic, Major Professor
Steve Carlson
Donald Sakaguchi

Iowa State University

Ames, Iowa

2011

"In order to do great things, a person must have a certain amount of intelligent ignorance."

Charles Kettering

TABLE OF CONTENTS

LIST OF FIGURES

LIST OF TABLES

THESIS ORGANIZATION

This thesis is organized into three major chapters: Chapter One, Chapter Two and Chapter Three. Chapter One contains an introduction, and a literature review of a compressive optic neuropathy (CON), with a focus on optical coherence tomography (OCT) and pattern evoked electroretinogram (pERG) as diagnostic tools for CON. The second chapter contains my research, presented in the form of a manuscript which is submitted to the journal *Investigative Ophthalmology and Visual Science*. Chapter three contains a general discussion of my results, general conclusions, and proposed future work. The thesis is concluded with a list of references followed by acknowledgments.

CHAPTER 1. GENERAL INTRODUCTION

Introduction

Compressive optic neuropathy (CON) is a form of neuropathy that occurs as a result of chronic or acute optic nerve compression. The clinical hallmark of the condition is an acute or chronic progression of visual field deficits, with frequently present permanent vision loss. Compressive optic neuropathy is a relatively rare, but rather severe condition, with a prevalence of about 4 cases per 1000 individuals each year in the United States [1]. It may occur at any age, although it is more common to develop in individuals above the age of thirty. In children, CON is typically caused by tumors such as rhabdomyosarcoma or optic nerve glioma[2].

Loss of vision as a result of CON is one of the few potentially reversible causes of blindness in human patient population. CON can result in permanent vision loss especially if optic nerve atrophy is evident at the time when the condition is diagnosed. However, if detected early enough, significant visual recovery may occur after surgical intervention (surgical decompression) in cases such as traumatic/hemorrhage induced CON, pituitary adenomas, and Graves' orbitopathy [3].

Orbital tumors and blunt trauma to the orbit followed by air or hemorrhage compression of the optic nerve are the frequent cause of CON in adult population. Other common causes of CON include meningiomas, pituitary macroadenomas, and aneurysms [4-8]. Also, CON can be caused by autoimmune inflammatory diseases like Grave's disease (Graves' orbitopathy), which is characterized by swelling of extraocular muscles due to autoimmune myositis resulting in exophthalmus [9].

Different techniques have been used over the years to alleviate clinical symptoms of CON, and they include surgical decompression[10], focal radiation[11-13], and endovascular interventional procedures[14]. Orbital tumors resulting in severe compression of the optic nerve and orbital structures can be surgically treated via transcranial approaches [15], transorbital approach and extraorbital approach, while anterior lesions are mostly treated via transorbital approaches[15-17]. Regardless of the selected treatment modality, the level of visual recovery is variable and cannot be well predicted in a significant percent of patients [3].

Studies have shown that the retinal nerve fiber layer (RNFL) is the most affected retinal structure in patients suffering from ischemic or compressive optic neuropathies[18-20]. RNFL thickness can be used as an objective and quantitative measure of remaining viable axonal tissue, and seems to be a valid predictor of visual recovery following surgical and medical treatments in CON patients[21]. Unfortunately, there has been a relative lack of a relevant and reproducible animal CON models, which mimic pathology observed in human patients, and could be used to obtain better understanding of the mechanisms associated with the structural and functional optic nerve damage in CON.

The goal of the research described in this thesis was to develop a large, reproducible animal model of CON, which mimics human clinical condition. We also wanted to evaluate a detailed temporal structural (RNFL) and functional (retinal ganglion cell activity) changes using optical coherence tomography (OCT) and pattern evoked electroretinography (pERG). The final goal of this study was to evaluate whether functional and structural imaging routines can be further modified with a goal of obtaining more predictive imaging parameters, which could be potentially used for improvement of diagnostic and treatment modalities in human patient population.

Literature review

Following a compressive optic nerve insult, the number of surviving retinal ganglion cells dictates the extent of visual function recovery [22-24]. Structural and functional diagnostic tools such as optical coherent tomography (OCT) and pattern electroretinography (pERG) allow early detection of abnormal thickness of the retinal nerve fiber layer (RNFL) and help detect early optic nerve functional deficits. This information can be effectively used to objectively quantify the severity of structural and functional optic nerve deficits in patients with a sudden history of vision loss, or patients with a history of progressive visual field deficits due to the development of CON.

Optic nerve decompression may result in a positive visual outcome particularly if vision loss is incomplete [8]. Several studies showed that preoperative visual function can serve as a good predictive tool for long-term preservation of vision following surgical decompression [3, 25, 26].

CAUSES OF COMPRESSIVE OPTIC NEUROPATHY

1) **Grave's Orbitopathy.**

Graves' orbitopathy or thyroid associated orbitopathy is probably the most frequent cause of CON, and it is usually manifested by decreased visual acuity, afferent pupillary light reflex defects and dyschromatopsia [9]. This condition results in mechanical compression of the optic nerve at the orbital apex secondary to hypertrophic or inflammatory changes of the extraocular muscles [25]. Graves' orbitopathy often results in the anterior globe

displacement as a result of orbital tissue swelling. The condition is also characterized by edema, eyelid retraction, and erythema[27]. It has been demonstrated that autoantibodies associated with this condition often target orbital fibroblast and extraocular muscle proteins resulting in an infiltration of inflammatory cells and development of the orbital tissue edema. [27]. Statistics show that Graves' orbitopathy has an annual incidence of 3 per 100,000 and 16 per 100,000 for men and women, respectively. A total of 3 – 5% of all Graves' orbitopathy patients can experience severe pain and development of corneal ulcers as a result of excessive corneal exposure due to exophthalmus [27]. The likelihood of developing a compressive optic neuropathy from Graves' opthalmopathy is most significantly correlated with the presence of deficits in extraocular motility and periorbital motility at the orbital apex[28]. Smoking has been shown to be a risk factor for the development and progression of this disorder and can potentially raise the incidence of the syndrome 7.7-folds [27, 29].

There are still some controversies about the mechanism of ophthalmopathy in Graves' disease. Jacobson and Gorman [30], reported that patients with ophthalmopathy may be hypothyroid, euthyroid, or hyperthyroid. However, most patients with euthyroid ophthalmopathy have elusive thyroid dysfunction and most patients who are hypothyroid have been treated for hyperthyroidism[31].

2) Tumors.

The external compression of optic nerve by orbital tumors is a relatively uncommon condition, but represents a potentially treatable cause of compressive optic neuropathy [32]. Optic nerve tumors, intra-orbital tumors, and intracranial expansions of the sphenoid bone may cause CON. Compression of the optic nerve at the orbital apex can also occur

as a result of expansion or enlargement of extraocular muscles similar to thyroid-associated orbitopathy.

The optic nerve can also be compressed by meningiomas confined to the optic nerve, or by orbital extension of intracranial tumors. Tumor induced CON is usually characterized by progressive, persistent loss of vision, and may be accompanied by ocular motility dysfunction. Magnetic resonance imaging (MRI) or computerized tomography (CT) are often used to diagnose the presence of orbital and intracranial tumors causing optic nerve compression, and are essential tools for facilitation of surgical optic nerve decompression and tumor removal [32].

3) Encephalocele.

An encephalocele is a protrusion of brain tissue through a congenital fissure in the skull with an incidence of 0.3 to 0.7 cases per 1000 births [33]. Frontal basal encephaloceles are congenital malformations in which brain parenchyma protrudes through a bony defect in the cribriform plate and sphenoid bone. This may be accompanied by midline facial defects and anomalous optic disc development[34]. Basal encephaloceles may produce unilateral or bilateral proptosis and loss of vision as a result of compressive optic neuropathy[35].

4) Trauma.

Traumatic insults may result in compressive optic neuropathy due to air or blood accumulation in the orbital space, swelling of the orbital tissues or compression of the optic nerve with fragments of fractured orbital bones. In cases of indirect optic nerve injury (especially closed head injury), compressive and shearing forces are transmitted to

the orbital optic canal and orbital apex following blunt head trauma to the fronto-temporal region of the cranium or the superior orbital rim [36]. The optic nerve dura can fuse with the periosteum of the bone within the canal, and since the optic nerve vasculature is pial, bruising and compression of the optic nerve may develop, resulting in a compartment syndrome. This can further worsen compressive insult due to the release of free oxygen radicals, a cycle of swelling and ischemia, and ultimately result in the irreversible damage to optic nerve axons [37, 38]. Joseph et al., conducted a clinical study involving 14 patients with acute, unilateral optic nerve injury after blunt head trauma, and demonstrated frequent development of compressive optic neuropathy. In this study, optic nerves were examined one week after injury, and an attempt to restore vision was done by extracranial optic decompression through an ipsilateral external ethmoidectomy. [39]. In another clinical study, the use of oxidized regenerated cellulose (ORC) in orbital surgery was reported as a cause of CON [40]. The condition developed as a result of retention of some ORC after surgery. Since ORC is often used in surgery to control bleeding, it can significantly expand as a result of blood absorption. Due to these properties, it is able to exert a considerable compressive force within an enclosed space, resulting in compressive optic neuropathy [41, 42].

Optic nerve compression, caused by aneurysms and hemorrhage are also known causes of acute and chronic visual loss [4, 6, 7]. Calvarial stenosis may also cause progressive optic neuropathy and are best treated with optic nerve decompression [43-50].

The mechanism by which CON causes impaired vision is still not well understood. It has been suggested that the ischemia of retinal ganglion cells, accumulation of toxic metabolites, abnormal transport of growth factors, demyelination, and disruption of action

potential conduction can be responsible for functional and structural optic nerve damage [9]. Studies done by Ress et al., in an acute model of CON showed that generation of free radical (oxidative radicals) is a rapid event after acute compression of the optic nerve, which may result in neurotoxic effects on the optic nerve[65].

DIAGNOSTIC STRATEGIES FOR COMPRESSIVE OPTIC NEUROPATHY

A) Optical coherence tomography

Optical coherence tomography (OCT) is a non-invasive imaging technology that can be used to obtain cross-sectional images of the retina and optic nerve [9], and it is particularly valuable for diagnosis of structural optic nerve deficits. This imaging technique uses low-coherence interferometry, and is able to provide detailed images of biological tissues, different retinal layers, and has 3-dimensional (3D) imaging capabilities with a discrimination resolution between 4-8 micrometers [51-56]. OCT has optical sectioning capability which are analogous to that of a confocal microscope [57], and the principle under which it operates is very similar to ultrasonic imaging (ultrasound B-mode). Although both OCT and ultrasound operate under the same principle and are both able to create cross-sectional pictures, ultrasound and OCT use sound and light respectively, to measure the echo time delay of the reflected and backscattered light [58].

Because of its ability to produce high-resolution images of retinal structures, OCT has become a very relevant tool in clinical and experimental studies for the diagnosis of optic

nerve and retinal diseases such as glaucoma, retinal detachment, macular edema, and ischemic and compressive optic neuropathies [39, 59, 60]. The latest generation of OCT equipment, spectral domain OCT (SD-OCT), can provide images with axial resolution of <5 microns and allows identification of individual cell bodies in different retinal layers [61]. In a study which characterized structural retina and optic nerve properties in CON patients , Monteiro et al., reported a decrease in macular and RNFL thickness using OCT [62]. In another study involving parachiasmal tumors, Danesh-Meyer et al., also used OCT to predict visual recovery following decompressive surgery. They noticed that preoperative RNFL thickness loss was associated with poorer visual acuity and visual field recovery post decompressive surgery. They concluded from this study that patients who have significant RNFL loss at the time of operation are less likely to have recovery of visual function post surgery [63].

Pattern Evoked Electroretinography (pERG)

Pattern electroretinography (pERG) is an electrophysiological method for measuring retinal ganglion cell (RGC) function [68]. By performing pERG recordings, RGC cell membrane electrical responses can be obtained, which are generated after retinal stimulation with a reversing white and black checkerboard pattern [69]. In pERG studies, the term latency describes the timing of the response (in milliseconds), while amplitude describes a magnitude of electrical response (measured in microvolts), [70]. Studies in which retrograde degeneration of retinal ganglion cells was induced by intraorbital section of the optic nerve, suggested that the integrity of ganglion and bipolar cells contribute to normal pattern ERG [71, 72].

Evaluation of RGC function using pERG provides an objective method for early diagnosis of compressive optic neuropathy, since early development of functional optic nerve deficits is manifested by reduction in pERG amplitudes [73]. Porciatti and Berger, independently demonstrated significant decrease in pERG amplitudes in different optic neuropathy cases [73].

It has been previously shown that pERG amplitudes can be decreased in the early stage of CON [74]. In a study, which evaluated early functional optic nerve changes in CON patients affected by Grave's disease, it has been demonstrated that pERG amplitude decrease is one of early indicators of optic nerve compression. Furthermore, decreased pERG amplitudes in this patient group correlated well with an increase in optic nerve diameter (which developed most likely due to ischemic swelling or compressive edema) when compared to control (healthy) patients [73].

In patients with pituitary tumor induced optic nerve compression at the chiasmal region, Ventura et al. demonstrated that pERG can be used as a very sensitive, reliable, and accurate method for the detection of optic nerve deficits prior and after decompressive surgery [75].

Evaluations of patients with optic neuritis, hereditary optic atrophy (HOA), traumatic optic neuropathy, and CON showed that pERG amplitude, nerve fiber layer thickness and optic nerve appearance during fundoscopy could be used as a prognostic factor for evaluating the extent of visual recovery[76]. A five year follow up study in optic neuropathy patients revealed failure of full visual recovery in one third of the patients who had decrease in pERG amplitude below noise level [76].

ANIMAL MODELS OF CON – REVIEW

Different animal species (cat, rabbit, dog, and rat) have been used to study effects of the acute and chronic compression on the optic nerve functional and structural parameters [64, 65, 77-79].

Ress et al.,[65] used a rat model to study the effects of acute nerve compression. The aim was to determine whether reperfusion-induced, oxygen-derived free radical injury occurs in peripheral nerves subject to acute compression in normal and chronically diabetic rats (streptozocin-induced diabetics).

Therapeutic agents, deferoxamine and lazaroid U74389F, were given at different time intervals in an attempt to reduce oxidative injury. The results obtained from this experiment showed blood flow to the nerve was significantly reduced by 75% due to compression with silastic tubing. In nerves from diabetes mellitus rats, blood flow improved although it failed to return to baseline after decompression (tubing release), whereas in nerves from non-diabetes mellitus nerves, perfusion returned to baseline.

In diabetes mellitus nerves, they noticed a significant increase in melonyldialdehyde levels from baseline following reperfusion as well as in non-diabetes mellitus nerves. Similarly, they observed an increase in glucose metabolism and cellular defense enzyme activity during nerve compression. However, enzyme activities in diabetes mellitus nerves tended to decline compared to non-diabetes mellitus nerves suggesting that diabetes mellitus nerves are unable to withstand reperfusion-induced metabolic stress. In reperfused diabetes mellitus nerves, deferoxamine and lazaroid U74389F significantly reduced malonyldialdehyde levels.

Using this model of acute nerve compression, the authors concluded that diabetic nerves were more susceptible to the free radical damage. They concluded that incomplete ischemia was created and that compressed peripheral nerves were susceptible to free radical damage (confirmed by increase lipid peroxidation and decreased antioxidant defenses).

In another study Babovic et al., evaluated the mechanism of ischemia/reperfusion injury in rabbit optic nerves after acute compression [64]. Acute compression was achieved by wrapping the optic nerve trunk with silastic tubing for 2 hours, followed by reperfusion period of 1 hour. An application of intravenous deferoxamine, (an iron chelator and antioxidant), demonstrated that inhibition of lipid peroxidation could potentially be a viable strategy for treatment of compressive optic nerve injury. Their studies suggest that the optic nerve is susceptible to ischemia/reperfusion injury following nerve compression.

Cai et al., [78] also used a rabbit model to study the pathological changes in the retina and optic nerve associated with intraorbital optic nerve damage. Chronic optic nerve compression was achieved by implanting a balloon into the orbital space, which was filled with contrast medium. The animals were evaluated for potential optic nerve damage 2, 4, and 8 weeks after compressive surgery.

They have demonstrated development of congestion and edema of the optic disk after 2 weeks, which completely resolved 8 weeks postoperatively. Histopathological examination showed decreased axonal number in the optic nerve. Immunohistochemistry data also showed that the number of apoptotic cells in the retinal ganglion cell layer

increased gradually and remained high by week 8, and positively correlated with compression time.

Clifford-Jones et al.,[80] studied the effects of chronic optic nerve compression in a cat model by surgically implanting an inflatable silicon rubber balloon in the orbital space. Twenty two cats were used in the experiment, 17 of which the optic nerve was compressed in an attempt to stimulate or mimic an expanding orbital tumor. The experiment lasted from 2 to 176 days.

Data from experimental animals showed that the nerves were narrowed at the site of contact with the balloon while histological examination showed significant abnormalities in optic nerve structures. Demyelination with either complete or partial loss of myelin sheath of the fibers from around intact axons, was observed within the first week of compression as the predominant pathological change. However, by week five, remyelination by oligodendrocytes had occurred in some axons despite the presence of the compressive implant. Nevertheless, they have noticed that the myelin sheath of the new internodes had an abnormal paranodal organization - they were atypically short and thin, while breakdown of some of the new internodes was also evident.

Toya et al., [79] have studied the effect of chiasmal compression using a dog model. To achieve chiasmal compression, a small balloon was surgically inserted into the subarachnoid space. The balloon was inflated to cause chiasmal compression by pouring warm water into the ballon through the infusion pump. In one animal, chiasmal compression was maintained for 5 minutes by inflating the balloon, which was followed by an immediate decompression.

They have demonstrated that even very short compression time (5 minutes) resulted in a decrease in visual evoked potentials. However, 30 minutes after decompression, visual evoked potential amplitudes started to recover and by minute 40, the amplitude reached near normal (preoperative control) levels.

Considering that there are no studies which describe in great detail functional and structural parameters in an experimental animal model of compressive optic neuropathy, our principal goal was to develop an inducible model of compressive optic neuropathy which could be effectively used to improve our understanding of this condition.

CHAPTER 2. FUNTIONAL AND STRUCTURAL OPTIC NERVE DEFICITS IN A CANINE MODEL OF COMPRESSIVE OPTIC NEURPOPATHY

*R.N. Nzokwe[1,3], *H. Kecova[1,3], E. Hernandez-Merino[1,3], K.N. Hamouche[1], M. Pryde[1], S.J. Jacobson[1], S.A. Park[1,] E. Alward[1], R.H. Kardon[2,3], T. Lazic[3], S.D. Grozdanic[1,3]

[1]Veterinary Clinical Sciences, Iowa State University, Ames, IA; [2]Ophthalmology and Visual Sciences, University of Iowa, Iowa City, IA; [3]Department of Veterans Affairs Center for Prevention and Treatment of Vision Loss, Iowa City, IA.

Corresponding Author:

Sinisa D. Grozdanic D.V.M., Ph.D., Dipl ACVO
Department of Veterinary Clinical Sciences
College of Veterinary Medicine - Iowa State University
1471 Vet. Med. Bldg.
Ames, 50010 IA, U.S.A.
e-mail: sgrozdan@iastate.edu
Phone: (515) 294-6712
Fax: (515) 294-7520

*Both authors equally contributed to presented work

This work was supported by the Department of Veterans Affairs Center for Prevention and Treatment of Vision Loss – Iowa City, Iowa, USA and Veterans Affairs RR&D Grant # C4702R

Word count: 5587

Number of figures: 12

Number of tables: 2

Keywords: compressive optic neuropathy; optic nerve; retinal ganglion cells; nerve fiber layer; optical coherence tomography; pattern electroretinography.

Abstract

Purpose: To evaluate functional and structural deficits in a canine model of compressive optic neuropathy (CON).

Methods: CON was induced in healthy beagles by implanting a silicone implant into the orbit and inducing optic nerve compression for 24 hours. Retinal nerve fiber layer (RNFL) thickness was evaluated using optical coherence tomography (OCT). Pattern electroretinography (pERG) was performed to evaluate retinal ganglion cell (RGC) function 10 minutes and 30, 90 and 180 days after CON induction.

Results: Optic nerve compression resulted in significant immediate pERG deficits (P50-N95=0.4±0.1μV; mean±SEM) when compared to control (6.2±0.4 μV; $p<0.0001$). Analysis of OCT scans in the *area centralis* immediately after compression showed significant increase in RNFL thickness in CON dogs (39.5±1.8 μm) when compared to control values (26.4±1.5 μm, $p<0.0001$). Increased *area centralis* RNFL thickness correlated significantly with pERG deficits ($r^2= 0.43$, $p=0.03$). Analysis of peripapillary RNFL showed significantly decreased thickness ($p=0.0098$), which did not correlate with pERG deficits. Analysis of *area centralis* showed progressive loss of RNFL thickness at 90 and 180 days post compression. PERG amplitudes showed significant recovery at 90 days post compression ($p<0.05$), but this effect was gone by 180 days. Full-field ERG recordings did not reveal deficits at any time.

Conclusions: CON resulted in initial thickening of *area centralis* RNFL, followed by progressive RNFL loss. Pattern ERG analysis showed significant temporary improvement in RGC function. Inclusion of large retinal blood vessel profile in peripapillary RNFL

analysis seems to decrease detection sensitivity and specificity for RNFL changes in early stages of compressive injury.

Introduction

Visual loss caused by compressive optic neuropathy (CON) is one of the few potentially reversible causes of blindness. Compression of the anterior visual pathway can be caused by tumors, trauma, aneurysms, or enlarged eye muscles due to Grave's thyroid orbitopathy[9]. Treatment options vary depending on the cause and may consist of surgical decompression[10], focal radiation[11-13], or endovascular interventional procedures[14]. With chronic optic nerve compression, visual deficits may progress and ultimately become permanent, while the amount of visual recovery can be highly unpredictable regardless of treatment modalities[3]. Lack of visual improvement can occur if surgical decompression is inadequate or if compressive optic neuropathy is not diagnosed and treated early enough in its course, resulting in the permanent structural neuronal loss. Furthermore, a significant percentage of patients may continue to lose their vision, despite initial postoperative improvements[3]. Ultimately, recovery of vision following successful decompression depends on the number of viable optic nerve axons that have been preserved[22, 62, 66]. If a large number of axons still remain then it is expected that return of visual function will be possible, provided that the compression is successfully relieved without further inducing damage by surgical or radiation procedure itself. Considering that surgical, radiation, and endovascular treatments for CON have associated risks (further visual loss, stroke, and mortality)[67], it is extremely important

to assess visual prognosis and signs preceding irreversible optic nerve damage before treatment is planned and initiated.

Traditionally, in depth understanding of pathological processes is obtained by studying animal models, which replicate in great detail spontaneously occurring pathological events in human clinical population. More advanced understanding of mechanisms responsible for the functional and structural optic nerve changes as a result of compressive insults is sparse due to the relative lack of experimental studies evaluating functional, structural and molecular properties in relevant animal models. It has been postulated that visual impairment in CON patients may be produced by conduction block of action potentials due to mechanical compression, demyelination, ischemia of the retinal ganglion cell axons or disrupted axonal transport of neurotransmitters, organelles (mitochondria), growth factors and metabolites[9]. Studies from experimental animal models demonstrated that acute optic nerve compression results in almost immediate generation of free oxidative radicals, which can have potential neurotoxic effects[64]. Experimental studies in cats with an inflatable orbital implant inducing CON demonstrated development of demyelination followed by remyelination, and development of pupil light reflex (PLR) deficits and axonal loss[80].

The principal purpose of this study was to develop a reproducible large animal model of CON, which can realistically mimic changes seen in human clinical population. We also wanted to perform a detailed functional and structural optic nerve characterization in acute and chronic stages of experimentally induced compressive injury using pattern electroretinography (pERG) and optical coherence tomography (OCT), with

a goal of providing detailed comparison between changes observed in this experimental animal model and previously published data from the human patient population.

Materials and methods

Animals:

All experimental procedures were conducted in accordance with the ARVO Statement for Use of Animals in Ophthalmic and Vision Research and were approved by the Iowa State University Committee on Animal Care.

Nineteen healthy adult intact female beagles (6 years old) were used for the study. Before enrolment in the study, complete ocular examination, including intraocular pressure evaluation, slit lamp biomicroscopy and indirect ophthalmoscopy, was performed on each animal to rule out the presence of any pre-existing ocular diseases.

Before each recording of structural and functional properties of the retina, pupils were dilated with topical 1% tropicamide (Tropicamide, Falcon Pharmaceuticals, Fort Worth, TX, USA) and 10% phenylephrine hydrochloride (Ak-dilateTM, Akorn Inc, Buffalo Grove, IL, USA) to assure standard recording conditions.

Induction of compressive optic neuropathy (CON) model

CON model was induced in 12 dogs by surgical implantation of custom-made silicone reservoir (Nagor LTD, Isle of Man, UK) into the left orbit. Total of seven additional animals served as non-operated controls for all functional and structural recordings.

Animals were pre-medicated with intramuscular hydromorphone hydrochloride (0.1mg/kg; Dilaudid®, Hospira, Inc., IL, USA) and acepromazine maleate (0.01mg/kg, Vedco, USA). Anesthesia was induced with intravenous administration of propofol (3-5mg/kg, Schering Plough Animal Health, USA) and maintained with 1.5-2.5% halothane (Halocarbon Laboratories, USA) in a mixture of 1:1 oxygen and nitrous oxide. Body temperature was maintained using a heating pad (T/Pump® Professional, Gaymar Industries Inc., NY, USA) and a heating blanket (Bair Hugger®, Arizant Healthcare Inc., MN, USA). Systolic, mean and diastolic blood pressures were recorded with oscillometric arterial blood pressure monitor (Cardell Veterinary Monitor, Model 9401, Paragon Medical Supply, FL, USA) every 5 minutes and maintained in physiological levels with constant intravenous drip of lactated ringer's solution (10 ml/kg for the first hour, 5 ml/kg further on). Heart rate, saturation of hemoglobin with oxygen, respiratory rate, inspired CO_2, end-tidal CO_2 and end-tidal concentration of halothane were constantly monitored (Datascope Multinex Plus anesthesia monitor, Absolute Medical Equipment, NY, USA). After induction of anesthesia, area around the left orbit and left side of the head was clipped and prepared for aseptic surgical procedure. Intravenous cefazolin (22 mg/kg; Cefazolin, Sandoz Inc., NJ, USA) was administered as a preventative antibiotic and the same dose was repeated every 2 hours throughout the procedure.

With animals in sternal recumbence, skin incision was made above the left eye, in the area of orbital ligament. Palpebral nerve was identified and where necessary, retracted with sterile umbilical tape to avoid its damage during the procedure. Orbital ligament was incised lengthwise to enable access to the retrobulbar space. Gelpi retractor was inserted into the incision to enable good visualization of the surgical site and custom made inflatable silicone implant (Nagor LTD, Isle of Man, UK) was introduced into the orbit,

directly behind the eye. The injection port of the implant was passed through the incision in the orbital ligament and under the skin of the forehead into the occipital area (Fig. 1), where it was fixed to the muscle fascia with absorbable monofilament suture (PDS 3-0, Ethicon, USA). Surgical incision was closed routinely. Post-operative analgesia and inflammation control was maintained with hydromorphone hydrochloride (0.1mg/kg BW) every 6-8 hours (as needed) for 3 days and carprofen (4 mg/kg BW) once daily for 7 days.

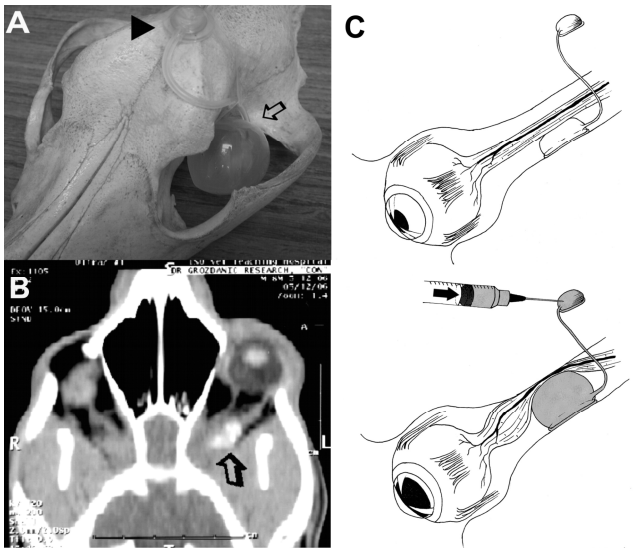

Figure 1: A) Positioning of the surgical implant is shown in a dog skull model- arrow points to the orbital implant, which is placed laterally and is inflated. Inflation of the implant results in the compression of the optic nerve against the medial orbital wall, since lateral orbital wall in canines is not completely encased with a bone. The arrowhead points to the injection port in the occipital region. **B)** Computerized tomography image of the surgical implant (arrow) in one of experimental animals. **C)** Schematic representation of the surgical implant placed in the orbit. Inflation of the device via subcutaneous port results in compression of the optic nerve. Saline can be injected or aspirated through the side port to control the level of optic nerve compression.

After insertion, the implant was inflated with 0.9% saline to induce 100% afferent pupil light reflex deficit (observed by illuminating operated eye and monitoring the control - non operated eye) using Melan 100 unit as previously reported[81]. The implant was deflated after 24h to mimic surgical optic nerve decompression by aspirating fluid via subcutaneous port.

Fluorescein angiography and optical coherence tomography recordings

Fluorescein angiography (FA) was performed to assure that perfusion of the retina and optic nerve was not significantly impaired by inflation of the implant (Fig. 2). Peripheral neuromuscular blockade was used to achieve stabile eye position in front of the FA camera (atracurium besylate, 0.2 mg/kg i.v., Bedford Laboratories, Bedford, OH, USA) and intermittent positive pressure ventilation (Multiflow 2002 anesthesia ventilator, Halowell EMC, Pittsfield, MA, USA) was established to provide respiratory support and maintain hemoglobin saturation with oxygen above 95% and end-tidal CO_2 at 35 - 45 mmHg. The level of paralysis was monitored using peripheral nerve stimulator (Microstim Plus, SunMed, Largo, FL, USA). Dogs were placed in sternal recumbence in front of the optical coherence tomograph equipped with fluorescein angiography module (SD-OCT; Heidelberg Engineering Spectralis OCT; Heidelberg Engineering, CA, USA; HRA/Spectralis Image Capture Module software version 1.1.0.0; Heidelberg Eye Explorer version 1.6.2.0), fluorescein (AK-Fluor 10%, Akorn, USA) was injected intravenously as a bolus (100 mg i.v. diluted in sterile saline solution to concentration 1:5) and the retinal blood vessel filling with fluorescein dye was observed and photographed (Fig. 2).

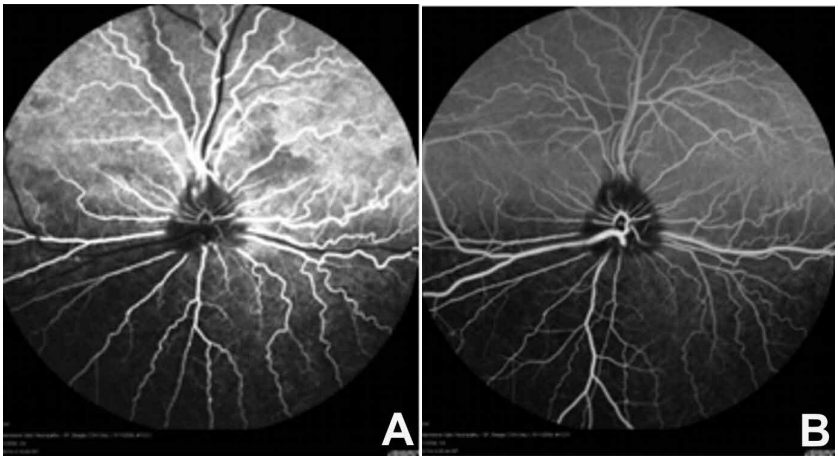

Figure 2. Fluorescein angiography was performed to confirm adequate retinal/optic nerve head perfusion after inflation of the implant. **A.** Arteriolar phase shows fluorescein filling of 15-20 arterioles (dogs do not have a central retinal artery), while dark unfilled veins are visible in the background; **B.** Venous phase of the fluorescein angiogram shows filling of the four major veins (dorsal, lateral, ventral and medial). Dogs do not have a central retinal vein. Some residual filling of arterioles can still be observed.

Evaluation of retinal and optic nerve structure using OCT was performed 10 minutes after implant inflation and 30, 90 and 180 days after surgery. Full retinal thickness, photoreceptor layer thickness and retinal nerve fiber layer (RNFL) thickness were evaluated using following OCT routines: peripapillary circle scan, horizontal volume scans through *area centralis* (region of the highest photoreceptor density) in the superio-temporal retina and a corresponding volume scan in the inferio-temporal retina. The peripapillary circle scan was used to evaluate the thickness of the peripapillary RNFL thickness in temporal, superior, nasal and inferior quadrant. The RNFL of peripapillary region was delineated using automated software (RNFL delineation was manually corrected where software's delineation was imprecise), while RNFL of *area centralis*

region and corresponding inferior retina was delineated manually, due to poor discrimination capability of automated software routines to delineate canine RNFL from these regions. The RNFL thickness of peripapillary circular scans was calculated for 4 quadrants (temporal, superior, nasal, inferior), and the results were compared to values from healthy (control, non-operated) beagles.

Functional recordings

Functional evaluation of retinal status using electroretinography was performed 10 minutes after implant inflation and 30, 90 and 180 days after surgery. Pattern electroretinogram (pERG) and full-field electroretinogram (ERG) were recorded to evaluate retinal electrical function (Roland Consult system, Brandenburg, Germany) as reported previously[82]. Briefly, pERG was recorded using 7 degrees checker-board pattern stimulus with a 2 Hz frequency, projected by a calibrated computer monitor from 20 cm distance from the eyes (low cut filter was set at 5 Hz, high cut filter was set at 50 Hz, retinal ganglion cell response was evaluated by measuring voltage between the P_{50}-N_{95} recording points by averaging 300 signals).

Full field ERG routines were recorded using Ganzfeld dome after 15 minute dark adaptation time. The standard flash intensity was 2 cds/m^2 = 0 log units. Maximum scotopic ERG responses were measured at 1.5 log unit (combined rod-cone response) with following amplification parameters: low cut amplifier frequency = 1 Hz; high cut amplifier frequency = 300 Hz, time interval between stimuli was 14.2 seconds (0.07 Hz), two responses were averaged. Photopic ERG was recorded using a 0.5 log unit background rod saturating illumination and 1.5 log unit cone flash stimulus (low cut amplifier frequency = 1 Hz; high cut amplifier frequency = 300 Hz, time interval between

stimuli was 5 seconds (0.2 Hz), 8 stimuli were averaged). Oscillatory potentials were recorded using 1.5 log unit flash stimulus (low cut amplifier frequency = 200 Hz; high cut amplifier frequency = 500 Hz, time interval between stimuli was 14.2 seconds (0.07 Hz), 8 stimuli were averaged). Photopic flicker was recorded using 0.5 log unit rod saturating illumination and 1.5 log units flickering flash stimulus at a frequency of 20Hz (low cut amplifier frequency = 1 Hz; high cut amplifier frequency = 300 Hz, 50 stimuli were averaged).

At the conclusion of the study (180 days after CON induction), animals were euthanized and eyes and optic nerves were collected and processed for histopathology evaluation.

Statistical analysis

Data analysis was performed using GraphPad (GraphPad Software, San Diego, California USA) as indicated in the text. A p value of <0.05 was considered significant.

Results

Acute functional and structural changes after 10 minutes of compression

Despite the evidence of relatively normal retina and optic nerve perfusion observed during fluorescein angiography, we have found significant changes in the structure and function of the retina and optic nerve immediately after the induction of compressive injury.

Structural evaluation of acute compressive changes (10 minutes post compression)

Optical coherence tomography revealed that RNFL thickness in *area centralis* region was significantly increased in CON dogs (39.5±1.9µm), when compared to healthy controls (26.4± 1.5µm, mean±SEM, Unpaired t-test, $p<0.0001$; Fig. 3).

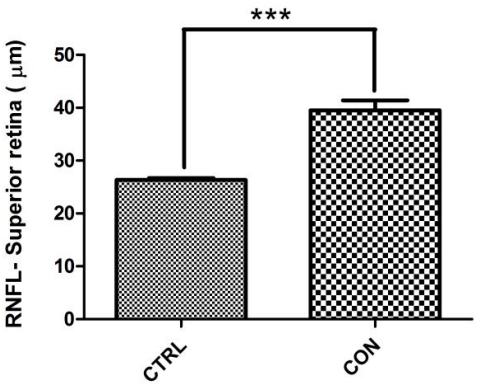

Figure 3: RNFL thickness in *area centralis* was significantly increased in CON dogs when compared to control dogs (CTRL) after 10 minutes of compression (Unpaired t-test, *** $p<0.0001$).

Contrary to RNFL thickness data obtained from the *area centralis* region, analysis of mean RNFL peripapillary thickness showed significant decrease (CON = 66.9 ± 3.6µm) after 10 minutes of optic nerve compression when compared to data from healthy control dogs (CTRL = 75.7± 1.3µm, $p<0.0098$, Unpaired t-test; Fig. 4A). When individual quadrants were compared between control and CON eyes, all quadrants had a trend toward decreased RNFL thickness, however decrease was statistically significant only in the ventral peripapillary quadrant ($p=0.0016$; Paired t-test; Fig. 4B).

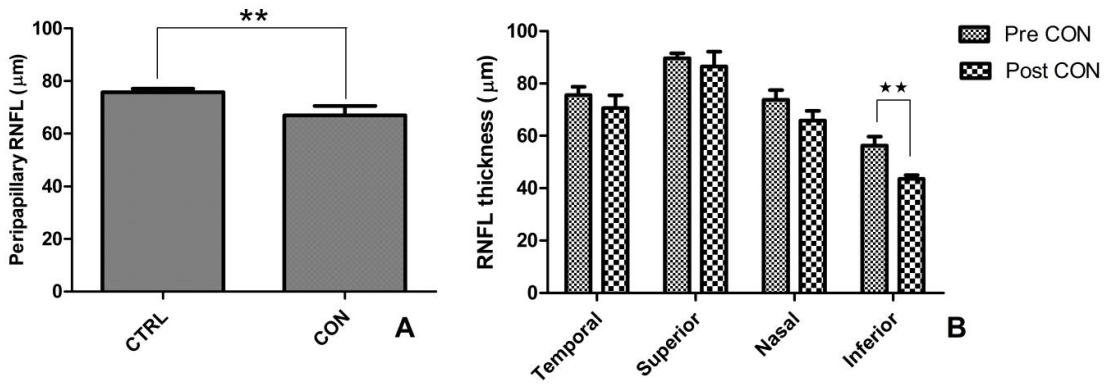

Figure 4: A. Mean peripapillary RNFL thickness after 10 minutes of compression was significantly decreased in CON dogs when compared to healthy controls (CTRL) ($p<0.0098$; Unpaired t-test, ** $p<0.01$). B. Peripapillary RNFL thickness before (pre CON) and 10 minutes after compression (post CON) – individual quadrants are shown: Temporal, Superior, Nasal and Inferior. RNFL thickness had a tendency to decrease in response to optic nerve compression in all quadrants, however, it was only significant in the inferior quadrant ($p=0.0016$; Paired t-test, ** $p<0.01$).

We hypothesized that this disproportion in compression-induced RNFL thickness between scans through *area centralis* (increased RNFL thickness) and peripapillary scans (decreased RNFL thickness) can be attributed to inclusion of the profile of large retinal blood vessels within the RNFL in the peripapillary scan analysis (Fig. 5). Therefore, we have analyzed the peripapillary RNFL thickness with exclusion of regions where large retinal blood vessels were embedded within the nerve fiber layer.

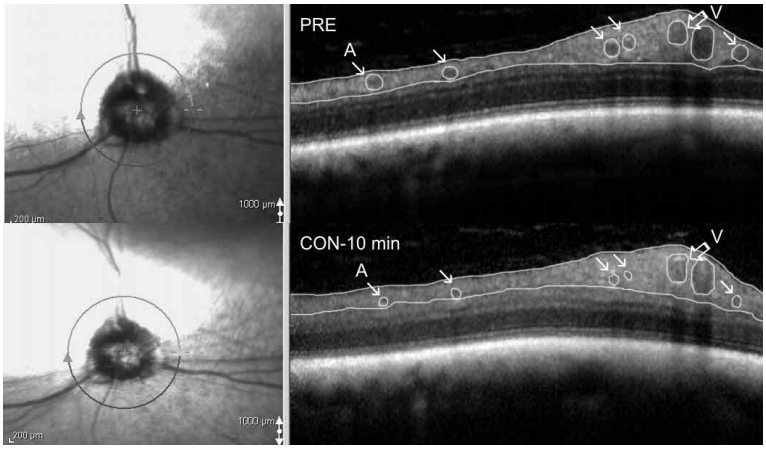

Figure 5: OCT peripapillary circle scan analysis from the same experimental animal revealed significant thinning of blood vessel profiles after CON induction (bottom image), when compared with the profile before compression (top image). Arrows mark arteries (A), open arrows mark veins (V).

Analysis of the peripapillary RNFL thickness after exclusion of blood vessels in the temporal quadrant (axonal bundles projecting to the *area centralis* region) showed significantly increased thickness (52.8 $\pm$ 4.0µm) when compared to the same area in healthy control dogs (45.3 $\pm$ 3.2µm, p = 0.0270, Unpaired t-test, Fig. 6B). Analysis of the inferior, nasal and superior quadrants showed a trend toward increased RNFL thickness, however difference was not statistically significant when compared to values from healthy (control) dogs (data not shown).

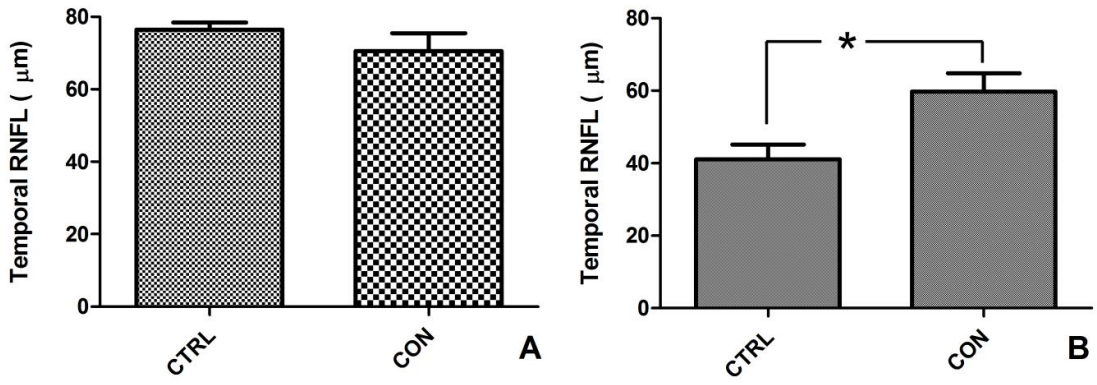

Figure 6: A) Analysis of temporal peripapillary RNFL thickness (area which receives majority of *area centralis* axonal bundles) with inclusion of blood vessels in the profile showed a tendency to decrease in CON dogs when compared to healthy control dogs. However, this was not statistically significant. **B)** Analysis of temporal peripapillary RNFL thickness after exclusion of blood vessels showed significant increase in the RNFL thickness of the temporal quadrant in CON dogs when compared to healthy control dogs (CTRL; p=0.0270; Unpaired t-test, * p<0.05).

Functional evaluation of acute compressive changes

Evaluation of pERG amplitudes showed significant decrease immediately after compression of the optic nerve (P_{50}-N_{95} = 0.4 $\pm$ 0.1µV) when compared to amplitudes in healthy control dogs (P_{50}-N_{95}= 6.2 $\pm$ 0.4µV; p<0.0001, Unpaired t-test).

Correlation analysis revealed a significant negative correlation between RNFL thickness in the *area centralis* and pERG amplitudes (r^2 = 0.4350, p = 0.0273; Fig. 7), which was highly suggestive of edematous RNFL changes contributing to the increased structural thickness observed during OCT analysis. However, correlation analysis of peripapillary temporal RNFL thickness (after blood vessel exclusion) did not show significant

correlation with pERG amplitudes (r^2 = 0.4620, p = 0.0663), despite this optic nerve region receiving majority of axons from the *area centralis* region. There was no correlation between peripapillary RNFL thickness (with exclusion of blood vessels) for inferior, nasal and superior quadrants and pERG amplitudes. No significant correlation was observed between peripapillary RNFL thickness (data including blood vessel profile) and pERG amplitudes for all evaluated segments (data not shown).

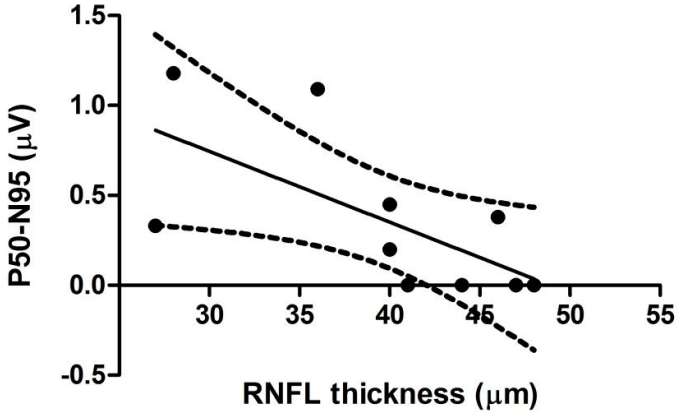

Figure 7: Statistical analysis showed significant negative correlation between pERG amplitudes (P_{50}-N_{95}) and RNFL thickness in the *area centralis* (r^2 = 0.4350, p = 0.0273; interrupted lines show 95% confidence interval).

<u>*Structural and functional analysis of chronic compressive changes*</u>

Structural analysis of chronic compressive changes

Retinal nerve fiber layer thickness was significantly decreased in the superior retina/*area centralis* (p<0.0001, One-way ANOVA; Fig. 8A) and corresponding inferior (p<0.0001, One-way ANOVA; Fig. 8B) retina when linear scans were analyzed.

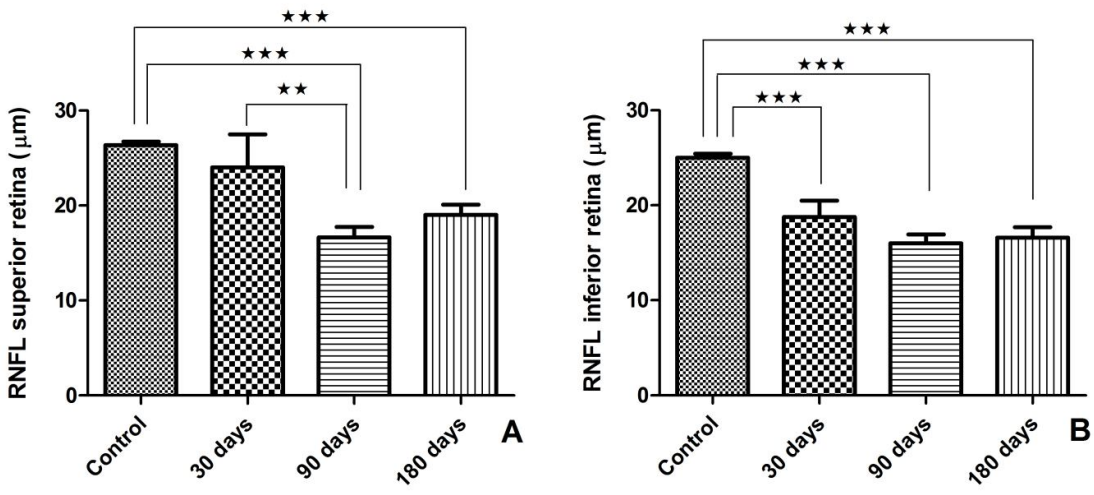

Figure 8. Analysis of RNFL thickness in the *area centralis* and corresponding inferior retina regions from linear scans. RNFL thickness was significantly decreased as a result of CON in superior and inferior retina. **A)** Superior retina (*area centralis*) RNFL analysis. **B)** Inferior retina RNFL analysis. (** $p<0.01$; *** $p<0.0001$)

Peripapillary RNFL thickness (without exclusion of blood vessels) was significantly decreased in temporal ($p=0.0002$, One-way ANOVA; Table 1), superior ($p=0.0002$, One-way ANOVA; Table 1), nasal ($p=0.0074$, One-way ANOVA; Table 1) and inferior ($p<0.0001$, One-way ANOVA; Table 1) quadrant. Analysis of the RNFL thickness for nasal quadrant showed statistically significant decrease in thickness at 180 days post compression, but not at 30 and 90 days post compression, despite the trend toward significant thinning at these time points.

Peripapillary scan - quadrant	Control	30 days	90 days	180 days
RNFL – C: temporal (µm)	76.44±2.1	**46.8±8.4 p<0.05**	**44.3±8.4 p<0.001**	**44.3±8.2 p<0.001**
RNFL – C: superior (µm)	91.3±1.6	**52.4±11.0 p<0.001**	**55.2±10.8 p<0.001**	**52.3±9.7 p<0.001**
RNFL – C: nasal (µm)	78.8±3.6	51.2±11.6 p>0.05	52.0±11.1 p>0.05	**51. 7±13.0 p<0.05**
RNFL – C: inferior (µm)	55.8±2.6	**31.4±2.8 p<0.0001**	**31.0±3.0 p<0.0001**	**30.5±4.5 p<0.0001**

Table 1: Peripapillary RNFL thickness analysis. Statistical analysis revealed significant decrease in RNFL thickness in all quadrants when compared to normal controls. Results of Bonferroni's post test (ANOVA) are shown for individual time points when compared with data from control (healthy) animals. Values are shown as mean ±SEM.

Total retinal thickness was significantly decreased in the superior (p=0.0133, One-way ANOVA) and inferior (p=0.0312, One-way ANOVA) retina (data not shown). Optical coherence tomography analysis did not reveal significant change in the outer nuclear layer (ONL) thickness in superior retina (*area centralis*) at any of recorded time points after CON induction (p=0.618, One-way ANOVA) when compared to values from healthy control dogs: 50.1±1.8 µm (CTRL), 54±3.9 µm (30d postoperatively), 50±1.9 µm (90d postoperatively) and 51.4±1.9 µm (180d postoperatively). Similar results were found for the ONL in the inferior retina (41.8±3.6 µm, 37.7±5 µm and 38±3.5 µm at 30, 90 and 180 days post CON induction respectively, CTRL= 44.3±1.1 µm; p=0.33, One-way ANOVA).

Functional analysis of chronic compressive changes

Compressive optic neuropathy resulted in significant and permanent RGC function loss observed by a decrease in pERG P_{50}-N_{95} amplitude ($p<0.0001$, One-way ANOVA, Fig. 9, 10). However, pattern ERG recordings showed rather dynamic changes throughout the experiment, with significant, but temporary partial recovery of RGC function 90 days after compressive injury ($p<0.05$, Bonferroni's post test; Fig. 9), despite the progressive development of the RNFL thickness loss (Fig. 8).

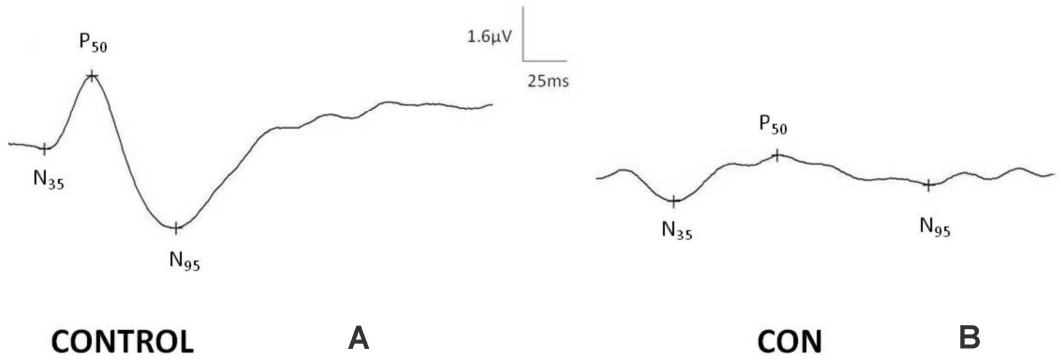

Figure 9. Pattern ERG recording 90 days after induction of CON. **A)** pERG tracing was recorded from the non-operated (CONTROL) eye; **B)** pERG tracing was recorded from the operated (CON) eye of the same experimental animal.

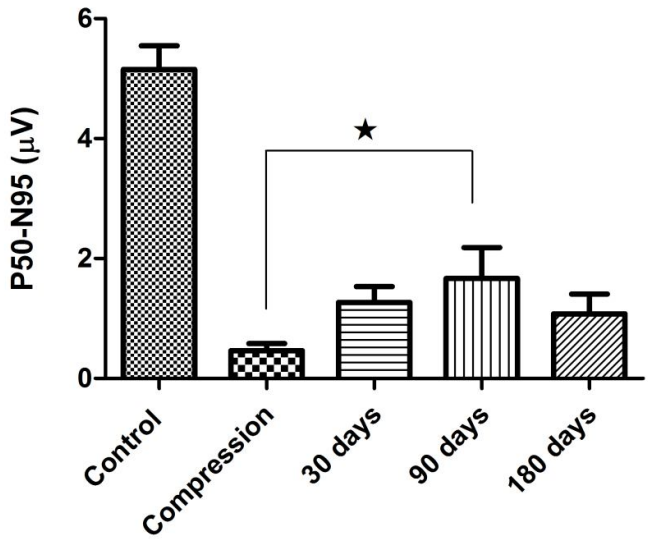

Figure 10. Pattern ERG analysis (P_{50}-N_{95} amplitude) showed significant decline in retinal ganglion cell function as a result of experimental optic nerve compression compared to control values. Post analysis (Bonferroni's test) demonstrated significant but temporary partial recovery of ganglion cell function at 90 days after compression, however that effect was lost at 180 days post compression (* $p<0.05$).

Full field ERG recordings showed well preserved amplitudes for all recorded routines: scotopic maximum response, scotopic oscillatory potentials, photopic response and photopic flicker (Fig. 11). Full field ERG analysis did not show a significant decrease of individual amplitudes over time in operated eyes when compared to non-operated (control) eyes for any of observed time points (Table 2). Histology analysis revealed the loss of large retinal ganglion cells and RNFL thinning (Fig. 12), confirming the validity of *in vivo* obtained RNFL thickness data using OCT analysis.

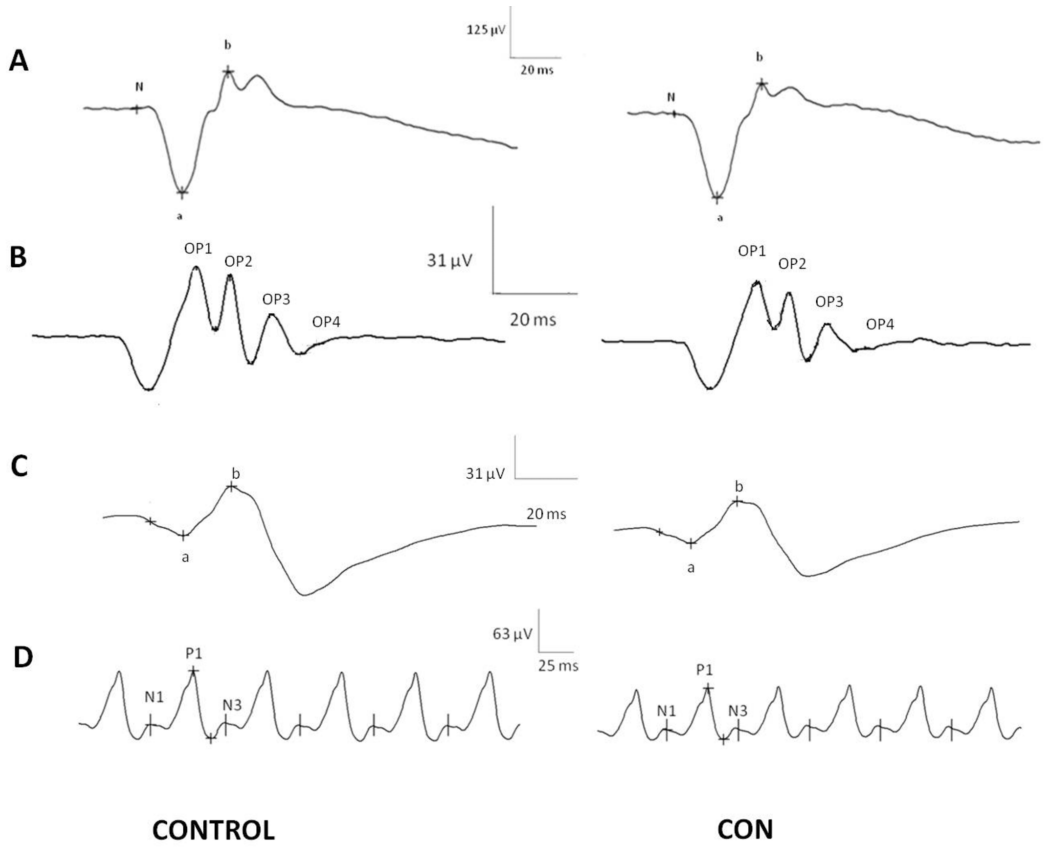

Figure 11. Full-field ERG recordings from a dog 90 days after induction of CON showed intact retinal electrical activity (pERG amplitudes of the same experimental animal are shown in Fig. 9). The left column represents recordings from the non-operated (CONTROL) eye, while the right column represents recordings from the operated (CON) eye of the same animal. A) Scotopic maximum response; B) Scotopic oscillatory potentials; C) Photopic cone response, and D) Photopic flicker.

	Control	30 days	90 days	180 days
Scotopic a-wave	102.5±4.6%	78.6±14.6%	94.0±23.6%	69.6±11.1%
Scotopic b-wave	106.7±2.6%	113.2±24.9%	78.2±11.2%	71.8±8.9%
Oscillatory potentials	92.5±4.2%	104.2±17.9%	83.2±10.9%	61.2±12.1%
Photopic a-wave	101.7±21.1%	91.0±35.4%	123.3±38.6%	124.7±21.7%
Photopic b-wave	97.0±4.5%	83.0±8.1%	96.8±18.6%	94.0±15.5%
Photopic flicker	101.7±2.9%	72.8±16.1%	81.7±16.7%	85.8±13.0%

Table 2. Full-field ERG analysis. Data is represented as a ratio between left (operated) and right (control) eyes. The second column (Control) shows ratio between left and right eyes for non-operated (control) healthy dogs. Statistical analysis did not show a significant difference in any of recorded parameters for CON dogs when compared to healthy (control) animals. Values are shown as mean ± SEM.

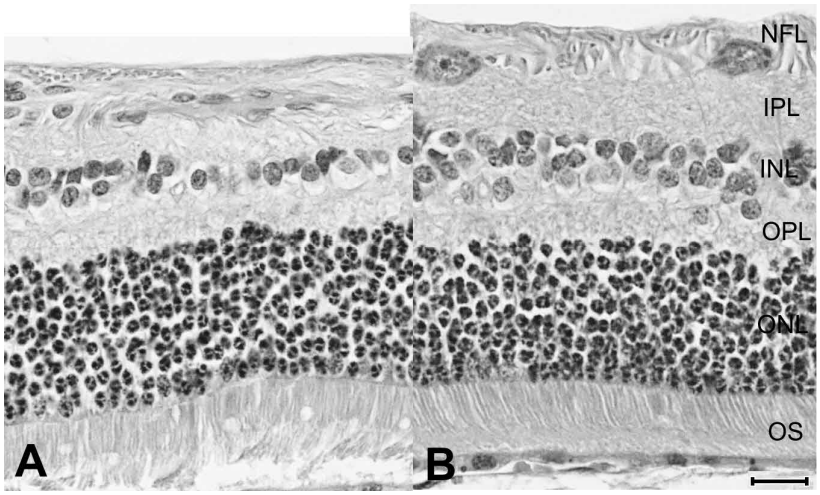

Figure 12. Histology analysis revealed retinal ganglion cell loss and nerve fiber layer thinning in CON eyes. A) CON retina 6 months post surgery; B) Control retina (NFL- nerve fiber layer, IPL - inner plexiform layer, INL - inner nuclear layer, OPL - outer plexiform layer, ONL - outer nuclear layer, OS - outer segments, bar = 10 μm)

Discussion

Compressive optic neuropathy is one of rare conditions where aggressive surgical and medical therapy can result in a partial or complete reversal of vision abnormalities[25]. Numerous studies in the field described strong presence of preoperative visual function as a good prognostic indicator for the long term vision preservation after decompression surgical procedures[3, 25, 83]. Chronic compressive lesions are usually characterized by a progressive or sudden loss of visual acuity, disturbances in color vision, anisocoria (due to afferent pupil light reflex defects), and/or decrease in electrophysiological optic nerve properties (observed by visual evoked potential or pERG deficits)[25, 84]. Considering that acute compressive lesions are

frequently associated with traumatic events[85-87], which are usually accompanied by a change in mentation or the complete loss of conscience, evaluation of the afferent pupil light reflex deficits is frequently employed as a quick screening test of the optic nerve function[9]. Several studies attempted to use more objective methods to evaluate optic nerve function and structure in CON patients, with a goal of obtaining objective predictive parameters for postoperative recovery of visual function. It has been demonstrated that preoperative presence of good peripapillary RNFL thickness (obtained by OCT analysis) in patients with pituitary adenomas is associated with better postoperative visual function, while the presence of thin RNFL was associated with poor postoperative visual outcomes[88]. Elegant studies by Monteiro et al demonstrated presence of structural (reduced macular and RNFL thickness) and functional (perimetry, pERG recordings) deficits in patients with compressive lesions[62], while Ventura et al demonstrated that pERG recordings can be used as a sensitive and objective method for detection of early optic nerve functional deficits and postoperative recovery associated with pituitary tumor compression of chiasmal region[75]. Similar results have been observed in studies which utilized VEP recordings for early detection of compressive optic nerve lesions and follow up of therapeutic outcomes[89, 90].

In this study we have demonstrated that compression of the optic nerve causing absolute afferent pupil light reflex deficits and relatively normal optic nerve and retinal perfusion, results in a dramatic and immediate decrease in RGC function evaluated by pERG recordings. Furthermore, we have shown that early compression results in the increased RNFL thickness in the *area centralis* (region corresponding to human macula), and this structural change had a significant negative correlation with pERG amplitudes. We hypothesize that increased RNFL thickness and decrease in RGC electrical properties,

was most likely caused by compression induced axoplasmatic stasis and ischemic swelling of the retinal ganglion cell axons, however the exact nature of observed functional and structural changes could not be precisely determined from our experimental results. The analysis of the peripapillary RNFL thickness (with inclusion of blood vessels in the calculated RNFL profile) had poor correlation with functional RGC status (pERG amplitudes). We have demonstrated that optic nerve compression is associated with some degree or blood vessel compression, which most likely resulted in the artificial RNFL "thinning" reported by automated software routines, due to the inclusion of blood vessels in the RNFL profile analysis. Based on data from this experimental model, we hypothesize that an objective analysis of the RNFL thickness using the OCT in acute CON patients has to be focused on the macular region, which has been already previously reported in different studies evaluating human CON patients[22, 66], while peripapillary RNFL thickness has to be critically evaluated by excluding the contribution of blood vessels from the RNFL thickness profile. Since retinal blood vessels contribute approximately 13% of the total peripapillary RNFL thickness in human retinas[91], it is possible that acute compressive change may result in similar RNFL "psudothinning", or even "normal" RNFL values in cases where calculation of RNFL thickness is a sum of edematous RNFL (increased thickness) and compressed blood vessels (decreased thickness). Considering that recent data showed that RNFL thinning is a poor prognostic indicator for the postoperative vision recovery[88], inaccurate evaluation of the RNFL thickness (presence of "pseudothinning" due to the inclusion of compressed blood vessels in the peripapillary RNFL thickness calculation) may guide clinical treatment toward less aggressive therapy, even in cases where RNFL may be relatively well preserved.

Analysis of chronic structural changes revealed progressive loss of the RNFL thickness which reached the lowest values at 90 days post compressive insult, and did not appear to further progress at later time point (180 days postoperatively). However, contrary to structural changes, functional evaluation of the RGC function revealed significant, but temporary recovery which progressed until 90 days post insult, and then declined at 180 days. While we do not have proper explanation for these late changes in functional RGC properties, we speculate that even severely damaged optic nerves have an intrinsic capacity to preserve function for a prolonged period of time after traumatic insult. We have previously observed development of spontaneous, but temporary functional recovery of optic nerve function in rodent models of acute elevation of intraocular pressure and laser-induced chronic ocular hypertension[92-94]. Dynamics of the functional recovery in rodent eyes have been observed 25-35 days after the insult, and correlated well with the intrinsic up-regulation of cilliary neurotrophic growth factor (CNTF)[92-94]. Whether similar type of events are present in canine CON eyes remains to be explored. The alternative explanation could be development of the remyelination process as previously described in a feline CON model[80]. However, decline in RGC functional properties at 180 days post injury observed in our study, is not supportive of the continuous optic nerve improvement which would be expected as a result of the remyelination process.

Development of the large animal CON model, which is characterized by progressive functional and structural optic nerve deficits in absence of other retinal layers abnormalities, may potentially allow for better understanding of molecular, functional and structural changes present in humans affected with similar conditions. Considering that the size of canine eye is similar to the human eye, it is likely that this model may allow

for effective development of novel imaging and therapeutic strategies, which could be easily translated to the human clinical population. Since CON is a relatively rare clinical condition, availability of reproducible animal model may allow for dramatic acceleration of our understanding of this type of injury in the future.

References

1. Sofferman, R.A., Harris P. Mosher Award thesis. The recovery potential of the optic nerve. Laryngoscope, 1995. **105**(7 Pt 3 Suppl 72): p. 1-38.
2. Acheson, J.F., Optic nerve disorders: role of canal and nerve sheath decompression surgery. Eye (Lond), 2004. **18**(11): p. 1169-74.
3. Cockerham, K.P. and S.S. Chan, Thyroid eye disease. Neurol Clin, 2010. **28**(3): p. 729-55.
4. Goda, J.S., et al., Long-term outcome in localized extranodal mucosa-associated lymphoid tissue lymphomas treated with radiotherapy. Cancer, 2010. **116**(16): p. 3815-24.
5. Chaudhry, I.A., et al., Orbital pseudotumor: distinct diagnostic features and management. Middle East Afr J Ophthalmol, 2008. **15**(1): p. 17-27.
6. Vargas, M.E., et al., Endovascular treatment of giant aneurysms which cause visual loss. Ophthalmology, 1994. **101**(6): p. 1091-8.
7. Bulters, D.O., et al., Visual recovery following optic nerve decompression for chronic compressive neuropathy. Acta Neurochir (Wien), 2009. **151**(4): p. 325-34.

8. Monteiro, M.L., et al., Correlation between macular and retinal nerve fibre layer Fourier-domain OCT measurements and visual field loss in chiasmal compression. Eye (Lond), 2010. **24**(8): p. 1382-90.

9. Monteiro, M.L., et al., Relationship between optical coherence tomography, pattern electroretinogram and automated perimetry in eyes with temporal hemianopia from chiasmal compression. Invest Ophthalmol Vis Sci, 2009. **50**(8): p. 3535-41.

10. Danesh-Meyer, H.V., et al., Relationship between retinal nerve fiber layer and visual field sensitivity as measured by optical coherence tomography in chiasmal compression. Invest Ophthalmol Vis Sci, 2006. **47**(11): p. 4827-35.

11. Foroozan, R., Chiasmal syndromes. Curr Opin Ophthalmol, 2003. **14**(6): p. 325-31.

12. Babovic, S., et al., Role of reactive oxygen species in optic nerve compression injury: a preliminary study. Ann Plast Surg, 1998. **40**(2): p. 156-9.

13. Clifford-Jones, R.E., W.I. McDonald, and D.N. Landon, Chronic optic nerve compression. An experimental study. Brain, 1985. **108 (Pt 1)**: p. 241-62.

14. Grozdanic, S.D., et al., Evaluation of retinal status using chromatic pupil light reflex activity in healthy and diseased canine eyes. Invest Ophthalmol Vis Sci, 2007. **48**(11): p. 5178-83.

15. Grozdanic, S.D., et al., Functional and structural changes in a canine model of hereditary primary angle-closure glaucoma. Invest Ophthalmol Vis Sci, 2010. **51**(1): p. 255-63.

16. Carter, K.D., et al., Long-term efficacy of orbital decompression for compressive optic neuropathy of Graves' eye disease. Ophthalmology, 1991. **98**(9): p. 1435-42.

17. Sleep, T.J., et al., Visual function following neurosurgical optic nerve decompression for compressive optic neuropathy. Eye (Lond), 2003. **17**(5): p. 571-8.

18. Spadea, L., et al., Early detection of P-VEP and PERG changes in ophthalmic Graves' disease. Graefes Arch Clin Exp Ophthalmol, 1997. **235**(8): p. 501-5.

19. Yazici, B. and T. Gonen, Posttraumatic subperiosteal hematomas of the orbit in children. Ophthal Plast Reconstr Surg, 2011. **27**(1): p. 33-7.

20. Zimmer-Galler, I.E. and G.B. Bartley, Orbital emphysema: case reports and review of the literature. Mayo Clin Proc, 1994. **69**(2): p. 115-21.

21. Linberg, J.V., Orbital compartment syndromes following trauma. Adv Ophthalmic Plast Reconstr Surg, 1987. **6**: p. 51-62.

22. Jacob, M., et al., Predicting visual outcome after treatment of pituitary adenomas with optical coherence tomography. Am J Ophthalmol, 2009. **147**(1): p. 64-70 e2.

23. Ventura, L.M., F.X. Venzara, 3rd, and V. Porciatti, Reversible dysfunction of retinal ganglion cells in non-secreting pituitary tumors. Doc Ophthalmol, 2009. **118**(2): p. 155-62.

24. Bobak, P., et al., Visual evoked potentials to multiple temporal frequencies. Use in the differential diagnosis of optic neuropathy. Arch Ophthalmol, 1988. **106**(7): p. 936-40.

25. Holder, G.E. and P.R. Bullock, Visual evoked potentials in the assessment of patients with non-functioning chromophobe adenomas. J Neurol Neurosurg Psychiatry, 1989. **52**(1): p. 31-7.

26. Hood, D.C., et al., Blood vessel contributions to retinal nerve fiber layer thickness profiles measured with optical coherence tomography. Journal of Glaucoma, 2008. **17**(7): p. 519-28.

27. Grozdanic, S.D., et al., Exogenous modulation of intrinsic optic nerve neuroprotective activity. Graefes Arch Clin Exp Ophthalmol, 2010. **248**(8): p. 1105-16.

28. Grozdanic, S.D., et al., Functional evaluation of retina and optic nerve in the rat model of chronic ocular hypertension. Exp Eye Res, 2004. **79**(1): p. 75-83.

29. Grozdanic, S.D., et al., Functional characterization of retina and optic nerve after acute ocular ischemia in rats. Invest Ophthalmol Vis Sci, 2003. **44**(6): p. 2597-605.

CHAPTER 3. GENERAL DISCUSSION

Discussion

We have developed a canine model of compressive optic nerve injury with a goal to investigate functional and structural optic nerve deficits following acute and chronic optic nerve compression. The effect of acute compression was studied 10 minutes post compression while chronic effects were studied 30, 90, and 180 days after compression. The advantage of an acute study is that it allowed us to evaluate very early changes in functional and structural retina and optic nerve parameters, which are usually observed with acute traumatic injuries. Chronic experiments allowed us to perform a detailed evaluation of changes associated with compressive optic nerve injury up to six months post compressive insult. Previous studies of CON have relied on the analysis of tissues obtained from sacrificed animals for their assessment of retinal and optic nerve damage. Techniques utilized in our studies allowed us the real time monitoring of physiological and morphological changes following compressive insult in the same animal over a long period of time, thus allowing us to precisely determine the range of dynamic changes developing after compressive optic nerve injuries.

Our results suggest that optic nerve compression results in an immediate impairment of retinal ganglion cell function, which is accompanied by changes in the profile of the RNFL thickness, supporting the notion than an immediate therapeutic intervention is a must in order to rescue any optic nerve axons that are functionally and structurally compromised by the compressive injury.

Considering that previous animal models of compressive optic nerve injury were characterized by significant ischemic changes, we have intentionally induced

compression, which caused significant functional impairments, but still provided relatively normal retina and optic nerve blood flow as observed by fluorescein angiography (intravenous injection of fluorescein dye) immediately after implant inflation.

Using a dog model of CON, we were able to show that despite relatively normal retina and optic nerve perfusion observed by fluorescein angiography after implant inflation, data obtained by OCT analysis showed that optic nerve compression results in an immediate and significant increase in RNFL thickness in the *area centralis* region (central retinal region with highest density of photoreceptors) with concurrent absence of afferent pupil light reflex. However, analysis of the peripapillary RNFL thickness (RNFL thickness around the entire optic nerve head), showed a significant decrease in RNFL thickness.

A substantial decrease in pERG amplitude (a measure of retinal ganglion cell electrical activity) was also noticed 15 minutes post compression, and correlation studies revealed a significant inverse relationship between increased *area centralis* RNFL thickness (most likely suggestive of RNFL edema) and pERG amplitudes. Nonetheless, the observed decrease in peripapillary RNFL thickness did not correlate with electrical amplitudes obtained from pERG recording. Previous studies in human CON patients have extensively evaluated the macular structural appearance (*area centralis* region in animals corresponds to the macular region in humans) and demonstrated similar pattern of changes as observed in our study [22-24]. In our study, we have demonstrated that the *area centralis* region in dogs is also immediately affected by the compressive insult. Based on our results, we hypothesize that an increase in *area centralis* RNFL thickness is probably caused by axoplasmatic stasis, ischemia, and swelling of retinal ganglion cell

axons as a result of the direct compressive insult on axonal structure, and likely component of ischemia which developed due to the partial compression of optic nerve vasculature.

A notion of possible ischemic component in our model has been supported by our data, which showed thinning (compression) of blood vessels embedded within the RNFL (Figure 5), despite relatively normal pattern of fluorescein angiography perfusion.

Consequently, we hypothesized that the decrease in peripapillary RNFL thickness could be potentially a consequence of compression induced thinning of blood vessels, whose profile is included in the calculation RNFL thickness.

Considering that blood vessels make up about 13% of peripapilary RNFL thickness in human retinas [95], it is very logical to hypothesize that any change in a diameter of retinal blood vessels, which we schematically represented in Figures A, B, and C, may affect the actual RNFL thickness values obtained during OCT measurements.

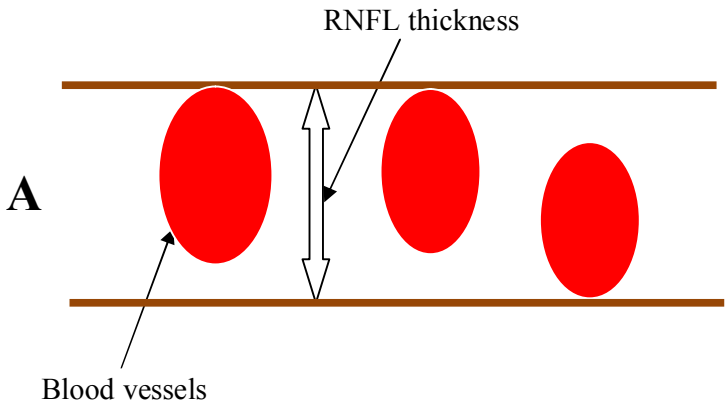

Figure 13: Normal retina with normal blood vessel size. OCT software analysis will report the actual thickness of the RNFL which includes blood vessel profile (double headed arrow).

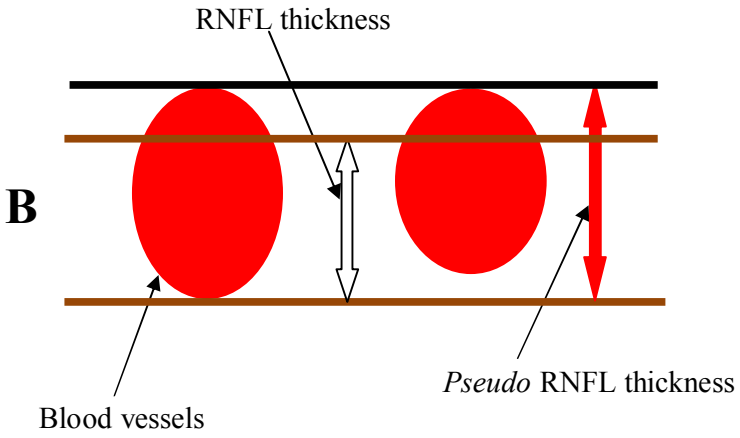

Figure 14: Normal retina with increased diameter of blood vessels (this kind of situation can be encountered with inflammatory diseases, which can cause vasodilatation). OCT software analysis may report an increase in RNFL thickness (red, double headed arrow) even though the actual RNFL thickness (clear, double headed arrow) in this case appears to be almost the same as in figure A.

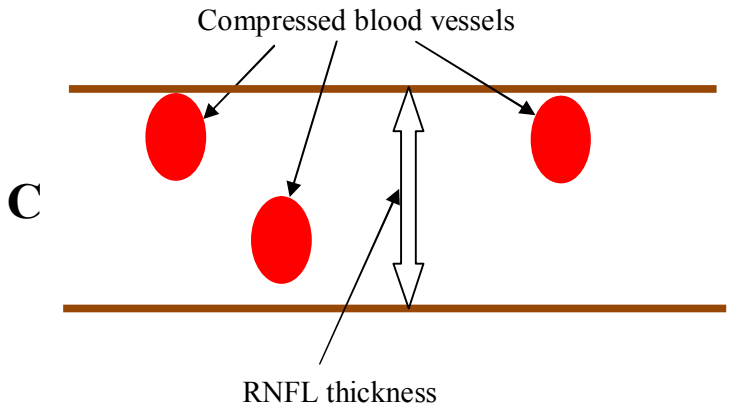

Figure 15: Schematic representation of proposed mechanism responsible for observed RNFL changes in our study. CON results in the compression of blood vessels and increased RNFL thickness due to axoplasmatic stasis and ischemic swelling of retinal ganglion cell axons. Because thin blood vessels are embedded within the RNFL, thinning of blood vessels can compensate for the real RNFL edema, and as a result the OCT software reports false normal or even false decreased (pseudothinning) RNFL thickness.

blood vessels. The results obtained from our analysis showed a trend toward an increase in the peripapillary RNFL thickness, in a similar manner as observed for the RNFL thickness in the *area centralis* region.

Analysis of chronic RNFL thickness change in our CON study by OCT showed a continuous decrease in RNFL thickness up to 90 days following compression, while there was no decrease at 180 days post compression. While structural evaluation showed a continuous RNFL decrease, data obtained by pERG analysis of RGC function showed a progressive recovery until day 90, followed by a dramatic decline of function 180 days post compression.

An explanation for the observed temporary improvement in retinal ganglion cell activity at day 90 is uncertain, but can be related to results obtained from rodent studies where dynamic functional recovery was seen 25-35 days after injury and was correlated with cilliary neurotrophic growth factor up-regulation [92-94].Also the change in retinal ganglion cell activity that we observed between days 90 and 180 may also be attributed to remyelination of axons as previously reported in a cat CON model [80].

Conclusion

We have successfully developed a large animal model (canine) of CON that reliably mimics changes observed in human clinical population. Considering that the size of canine eye is comparable to the human eye, this model can be used to further improve our understanding of CON as a relatively uncommon condition. Acute CON results in an immediate RNFL swelling, which is accompanied by decrease in RGC function. Furthermore, we have demonstrated that inclusion of blood vessels in the RNFL thickness may be potentially misleading when evaluating the status of the RNFL. These observations are likely to be very important when evaluating human patients, since decision to pursue more or less aggressive medical or surgical therapy is frequently based upon the RNFL status observed by OCT analysis.

Future work

We do have a unique opportunity to significantly increase our understanding of functional, structural and molecular events responsible for neuronal death as a result of compressive optic nerve injury. Considering the importance of OCT based routines during the decision process about aggressiveness of medical and/or surgical therapy for CON patients, it will be very important to develop software analysis routines which can realistically evaluate true RNFL properties, with exclusion of blood vessels. Since we (and others) have shown that OCT reported RNFL thickness can be significantly influenced by non-neuronal tissue components (glial proliferation, inclusion of blood vessels in the analysis routines), it is likely that novel OCT data analysis which will address influence of these factors on RNFL thickness evaluation will have to be developed in the future.

REFERENCES

1. Schiefer U, W.H., Hart W., Neuro-ophthalmic presentations of orbital disease. Clinical Neuro-Ophthalmology: A Practical Guide, 2007(Wien & New York: Springer).
2. Shields AJ, S.C., Scartozzi R., Survey of 1264 patients with orbital tumors and simulating lesions: the 2002 Montgomery Lecture, Part 1. Ophthalmology, 2004(111(5)): p. 997-1008.
3. Bulters, D.O., et al., Visual recovery following optic nerve decompression for chronic compressive neuropathy. Acta Neurochir (Wien), 2009. **151**(4): p. 325-34.
4. Cook, M.W., et al., Traumatic optic neuropathy. A meta-analysis. Arch Otolaryngol Head Neck Surg, 1996. **122**(4): p. 389-92.
5. Li, K.K., et al., Optic nerve decompression for compressive neuropathy secondary to neoplasia. Arch Otolaryngol Head Neck Surg, 1997. **123**(4): p. 425-9.
6. Long, D.M., Neurosurgical involvement in tumors of the orbit. Clin Neurosurg, 1985. **32**: p. 514-23.
7. Orzincolo C, B.P., Tamarozzi R, et al, Il cranio nell'osteodistrofia renale. Radio Med, 1987. **73**: p. 518-522.
8. Schmidt, R.H., et al., Compressive optic neuropathy caused by renal osteodystrophy. Case report. J Neurosurg, 2001. **95**(4): p. 704-9.
9. Sofferman, R.A., Harris P. Mosher Award thesis. The recovery potential of the optic nerve. Laryngoscope, 1995. **105**(7 Pt 3 Suppl 72): p. 1-38.

10. Acheson, J.F., Optic nerve disorders: role of canal and nerve sheath decompression surgery. Eye (Lond), 2004. **18**(11): p. 1169-74.

11. Cockerham, K.P. and S.S. Chan, Thyroid eye disease. Neurol Clin, 2010. **28**(3): p. 729-55.

12. Goda, J.S., et al., Long-term outcome in localized extranodal mucosa-associated lymphoid tissue lymphomas treated with radiotherapy. Cancer, 2010. **116**(16): p. 3815-24.

13. Chaudhry, I.A., et al., Orbital pseudotumor: distinct diagnostic features and management. Middle East Afr J Ophthalmol, 2008. **15**(1): p. 17-27.

14. Vargas, M.E., et al., Endovascular treatment of giant aneurysms which cause visual loss. Ophthalmology, 1994. **101**(6): p. 1091-8.

15. Margalit, N., et al., Orbital tumors treated using transcranial approaches: surgical technique and neuroophthalmogical results in 41 patients. Neurosurg Focus, 2007. **23**(5): p. E11.

16. Bejjani, G.K., et al., A reappraisal of surgery for orbital tumors. Part I: extraorbital approaches. Neurosurg Focus, 2001. **10**(5): p. E2.

17. Boulos, P.T., et al., Meningiomas of the orbit: contemporary considerations. Neurosurg Focus, 2001. **10**(5): p. E5.

18. Chai, S.J. and R. Foroozan, Decreased retinal nerve fibre layer thickness detected by optical coherence tomography in patients with ethambutol-induced optic neuropathy. Br J Ophthalmol, 2007. **91**(7): p. 895-7.

19. Miyahara, T., et al., Alterations in retinal nerve fiber layer thickness following indirect traumatic optic neuropathy detected by nerve fiber analyzer, GDx-N. Am J Ophthalmol, 2003. **136**(2): p. 361-4.

20. Predoi, D.V., et al., [Assessment of compressive optic neuropathy in hipofizar tumors]. Oftalmologia, 2008. **52**(4): p. 110-7.

21. Danesh-Meyer, H.V., et al., In Vivo Retinal Nerve Fiber Layer Thickness Measured by Optical Coherence Tomography Predicts Visual Recovery after Surgery for Parachiasmal Tumors. Investigative Ophthalmology & Visual Science, 2008. **49**(5): p. 1879-1885.

22. Monteiro, M.L., et al., Correlation between macular and retinal nerve fibre layer Fourier-domain OCT measurements and visual field loss in chiasmal compression. Eye (Lond), 2010. **24**(8): p. 1382-90.

23. Monteiro, M.L.R., et al., Relationship between Optical Coherence Tomography, Pattern Electroretinogram and Automated Perimetry in Eyes with Temporal Hemianopia from Chiasmal Compression. Investigative Ophthalmology & Visual Science, 2009. **50**(8): p. 3535-3541.

24. Danesh-Meyer, H.V., et al., Relationship between Retinal Nerve Fiber Layer and Visual Field Sensitivity as Measured by Optical Coherence Tomography in Chiasmal Compression. Investigative Ophthalmology & Visual Science, 2006. **47**(11): p. 4827-4835.

25. Carter, K.D., et al., Long-term efficacy of orbital decompression for compressive optic neuropathy of Graves' eye disease. Ophthalmology, 1991. **98**(9): p. 1435-42.

26. Sleep, T.J., et al., Visual function following neurosurgical optic nerve decompression for compressive optic neuropathy. Eye, 0000. **17**(5): p. 571-578.

27. Bahn, R.S., Graves' Ophthalmopathy. New England Journal of Medicine, 2010. **362**(8): p. 726-738.

28. Toussaint, P., et al., [Aspects of the tilted disk syndrome]. Bull Soc Ophtalmol Fr, 1989. **89**(2): p. 267-8, 271-2.

29. Giuffre, G. and M. Anastasi, Electrofunctional features of the tilted disc syndrome. Doc Ophthalmol, 1986. **62**(3): p. 223-30.

30. Jacobson DH, G.C., Endocrine Ophthalmopathy: Current ideas concerning etiology, pathogenesis, and treatment. Endocr Rev 5:200, 1984.

31. Brent, G.A., Graves' Disease. New England Journal of Medicine, 2008. **358**(24): p. 2594-2605.

32. Rootman, J., Diseases of the orbit. Philadelphia: JP Lippincott, 1988: p. 243-4.

33. Hershewe, G.L., et al., Optic nerve compression from a basal encephalocele. J Neuroophthalmol, 1995. **15**(3): p. 161-5.

34. Suwanwela, C. and C. Hongsaprabhas, Fronto-ethmoidal encephalomeningocele. J Neurosurg, 1966. **25**(2): p. 172-82.

35. Monica, M.L., E.S. Connolly, and R.F. Kalil, Basal encephalocele presenting with monocular visual loss. J Clin Neuroophthalmol, 1984. **4**(1): p. 9-13.

36. Anderson RL, P.W., Gross CE, Optic nerve blindness following blunt forehead trauma. Ophthalmology 1982(89): p. 445–455.

37. Steinsapir, K.D. and R.A. Goldberg, Traumatic optic neuropathy. Surv Ophthalmol, 1994. **38**(6): p. 487-518.

38. Tongabay Cumurcua, S.D., Soner Demirela, Cem Cankayaa, Traumatic Optic Neuropathy and Central Retinal Artery Occlusion Following Blunt Ocular Trauma. J Clin Med Res, 2011. **3**(1): p. 55-57.

39. Thomas, D. and G. Duguid, Optical coherence tomography--a review of the principles and contemporary uses in retinal investigation. Eye (Lond), 2004. **18**(6): p. 561-70.

40. Arat, Y.O., et al., Compressive Optic Neuropathy after Use of Oxidized Regenerated Cellulose in Orbital Surgery: Review of Complications, Prophylaxis, and Treatment. Ophthalmology, 2006. **113**(2): p. 333-337.

41. Dutton, J.J., D.T. Tse, and R.L. Anderson, Compressive optic neuropathy following use of intracranial oxidized cellulose hemostat. Ophthalmic Surg, 1983. **14**(6): p. 487-90.

42. Arat, Y.O., et al., Compressive optic neuropathy after use of oxidized regenerated cellulose in orbital surgery: review of complications, prophylaxis, and treatment. Ophthalmology, 2006. **113**(2): p. 333-7.

43. Al-Mefty, O., et al., Optic nerve decompression in osteopetrosis. J Neurosurg, 1988. **68**(1): p. 80-4.

44. Bland, L.I., M.J. Marchese, and J.V. McDonald, Acute monocular blindness secondary to fibrous dysplasia of the skull: a case report. Ann Ophthalmol, 1992. **24**(7): p. 263-6.

45. Donoso, L.A., L.E. Magargal, and R.A. Eiferman, Fibrous dysplasia of the orbit with optic nerve decompression. Ann Ophthalmol, 1982. **14**(1): p. 80-3.

46. Finney, H.L. and T.S. Roberts, Fibrous dysplasia of the skull with progressive cranial nerve involvement. Surg Neurol, 1976. **6**(6): p. 341-3.

47. Guyer, D.R., et al., Visual function following optic canal decompression via craniotomy. J Neurosurg, 1985. **62**(5): p. 631-8.

48. Nanami, T., et al., [Orbito-cranial reconstruction and unilateral optic canal release in a patient with left fronto-orbital fibrous dysplasia: a case report]. No Shinkei Geka, 1994. **22**(10): p. 967-71.

49. Norrdin, R.W., Fibrous osteodystrophy with facial hyperostosis in a dog with renal cortical hypoplasia. Cornell Vet, 1975. **65**(2): p. 173-86.

50. Weisman, J.S., R.S. Hepler, and H.V. Vinters, Reversible visual loss caused by fibrous dysplasia. Am J Ophthalmol, 1990. **110**(3): p. 244-9.

51. Drexler, W., et al., Ultrahigh-resolution ophthalmic optical coherence tomography. Nat Med, 2001. **7**(4): p. 502-507.

52. Drexler, W., et al., Enhanced Visualization of Macular Pathology With the Use of Ultrahigh-Resolution Optical Coherence Tomography. Arch Ophthalmol, 2003. **121**(5): p. 695-706.

53. Fujimoto, J.G., Optical coherence tomography for ultrahigh resolution in vivo imaging. Nat Biotech, 2003. **21**(11): p. 1361-1367.

54. Fujimoto, J.G., et al., Optical coherence tomography: an emerging technology for biomedical imaging and optical biopsy. Neoplasia, 2000. **2**(1-2): p. 9-25.

55. Wojtkowski, M., et al., Three-dimensional retinal imaging with high-speed ultrahigh-resolution optical coherence tomography. Ophthalmology, 2005. **112**(10): p. 1734-46.

56. Wojtkowski, M., et al., Ultrahigh-resolution, high-speed, Fourier domain optical coherence tomography and methods for dispersion compensation. Opt Express, 2004. **12**(11): p. 2404-22.

57. Davidovits, P. and M.D. Egger, Scanning Laser Microscope for Biological Investigations. Appl. Opt., 1971. **10**(7): p. 1615-1619.

58. Huang, D.S., Eric A.; Lin, Charles P.; Schuman, Joel S.; Stinson, William G.; Chang, Warren; Hee, Michael R.; Flotte, Thomas; Gregory, Kenton; Puliafito, Carmen A.; Fujimoto, James G., Optical Coherence Tomography. Science. **254**(5035): p. 1178-1181.

59. Gekeler, F., et al., Assessment of the posterior segment of the cat eye by optical coherence tomography (OCT). Vet Ophthalmol, 2007. **10**(3): p. 173-8.

60. Grozdanic, S.D., et al., Recovery of canine retina and optic nerve function after acute elevation of intraocular pressure: implications for canine glaucoma treatment. Veterinary Ophthalmology, 2007. **10**: p. 101-107.

61. Drexler, W., Ultrahigh-resolution optical coherence tomography. J Biomed Opt, 2004. **9**: p. 47-74.

62. Monteiro, M.L., et al., Relationship between optical coherence tomography, pattern electroretinogram and automated perimetry in eyes with temporal hemianopia from chiasmal compression. Invest Ophthalmol Vis Sci, 2009. **50**(8): p. 3535-41.

63. Danesh-Meyer, H.V., et al., In vivo retinal nerve fiber layer thickness measured by optical coherence tomography predicts visual recovery after surgery for parachiasmal tumors. Invest Ophthalmol Vis Sci, 2008. **49**(5): p. 1879-85.

64. Babovic, S., et al., Role of reactive oxygen species in optic nerve compression injury: a preliminary study. Ann Plast Surg, 1998. **40**(2): p. 156-9.

65. Ress, A.M., et al., Free radical damage in acute nerve compression. Ann Plast Surg, 1995. **34**(4): p. 388-95.

66. Danesh-Meyer, H.V., et al., Relationship between retinal nerve fiber layer and visual field sensitivity as measured by optical coherence tomography in chiasmal compression. Invest Ophthalmol Vis Sci, 2006. **47**(11): p. 4827-35.

67. Foroozan, R., Chiasmal syndromes. Curr Opin Ophthalmol, 2003. **14**(6): p. 325-31.

68. Oner, A., et al., Pattern Electroretinographic Recordings in Eyes With Myopia. Eye & Contact Lens, 2009. **35**(5): p. 238-241 10.1097/ICL.0b013e3181b343d9.

69. Heckenlively, J.R., & Arden, G. B., Princeples and practice of clinical electrophisiology of vision. 1991, Mosby Year Book.: USA.

70. Güven, A. and S. Kara, Diagnosis of the macular diseases from pattern electroretinography signals using artificial neural networks. Expert Systems with Applications, 2006. **30**(2): p. 361-366.

71. Maffei, L., et al., Pattern ERG in the monkey after section of the optic nerve. Experimental Brain Research, 1985. **59**(2): p. 423-425.

72. Hollander, H., et al., Electroretinographic responses and retrograde changes of retinal morphology after intracranial optic nerve section. A quantitative analysis in the cat. Exp Brain Res, 1984. **55**(3): p. 483-93.

73. Genovesi-Ebert, F., et al., Standardized echography, pattern electroretinography and visual-evoked potential and automated perimetry in the early diagnosis of Graves' neuropathy. Ophthalmologica, 1998. **212 Suppl 1**: p. 101-3.

74. Buzzonetti L, F.B., Tamburelli C, Cefala FM, Piccardi M, Grossi MG, L'elettroretinogramma da pattern nella neuropatie ottiche compressive. Atti VII Congr SIEO, Padova, 1992.

75. Ventura, L.M., F.X. Venzara, 3rd, and V. Porciatti, Reversible dysfunction of retinal ganglion cells in non-secreting pituitary tumors. Doc Ophthalmol, 2009. **118**(2): p. 155-62.

76. Kaufman, D.I., et al., The pattern electroretinogram: a long-term study in acute optic neuropathy. Neurology, 1988. **38**(11): p. 1767-74.

77. Clifford-Jones, R.E., W.I. McDonald, and D.N. Landon, Chronic Optic Nerve Compression An Experimental Study. Brain, 1985. **108**(1): p. 241-262.

78. Cai, J., et al., Pathologic changes in chronic intraorbital optic nerve damage in rabbits. Brain Research, 2009. **1267**: p. 103-115.

79. Toya, S., et al., Transsphenoidal exposure of the optic chiasm and a chiasmal compression model in the dog. A technical note. Keio J Med, 1982. **31**(1-2): p. 1-6.

80. Clifford-Jones, R.E., W.I. McDonald, and D.N. Landon, Chronic optic nerve compression. An experimental study. Brain, 1985. **108 (Pt 1)**: p. 241-62.

81. Grozdanic, S.D., et al., Evaluation of retinal status using chromatic pupil light reflex activity in healthy and diseased canine eyes. Invest Ophthalmol Vis Sci, 2007. **48**(11): p. 5178-83.

82. Grozdanic, S.D., et al., Functional and structural changes in a canine model of hereditary primary angle-closure glaucoma. Invest Ophthalmol Vis Sci, 2010. **51**(1): p. 255-63.

83. Sleep, T.J., et al., Visual function following neurosurgical optic nerve decompression for compressive optic neuropathy. Eye (Lond), 2003. **17**(5): p. 571-8.

84. Spadea, L., et al., Early detection of P-VEP and PERG changes in ophthalmic Graves' disease. Graefes Arch Clin Exp Ophthalmol, 1997. **235**(8): p. 501-5.

85. Yazici, B. and T. Gonen, Posttraumatic subperiosteal hematomas of the orbit in children. Ophthal Plast Reconstr Surg, 2011. **27**(1): p. 33-7.

86. Zimmer-Galler, I.E. and G.B. Bartley, Orbital emphysema: case reports and review of the literature. Mayo Clin Proc, 1994. **69**(2): p. 115-21.

87. Linberg, J.V., Orbital compartment syndromes following trauma. Adv Ophthalmic Plast Reconstr Surg, 1987. **6**: p. 51-62.

88. Jacob, M., et al., Predicting visual outcome after treatment of pituitary adenomas with optical coherence tomography. Am J Ophthalmol, 2009. **147**(1): p. 64-70 e2.

89. Bobak, P., et al., Visual evoked potentials to multiple temporal frequencies. Use in the differential diagnosis of optic neuropathy. Arch Ophthalmol, 1988. **106**(7): p. 936-40.

90. Holder, G.E. and P.R. Bullock, Visual evoked potentials in the assessment of patients with non-functioning chromophobe adenomas. J Neurol Neurosurg Psychiatry, 1989. **52**(1): p. 31-7.

91. Hood, D.C., et al., Blood vessel contributions to retinal nerve fiber layer thickness profiles measured with optical coherence tomography. Journal of Glaucoma, 2008. **17**(7): p. 519-28.

92. Grozdanic, S.D., et al., Exogenous modulation of intrinsic optic nerve neuroprotective activity. Graefes Arch Clin Exp Ophthalmol, 2010. **248**(8): p. 1105-16.

93. Grozdanic, S.D., et al., Functional evaluation of retina and optic nerve in the rat model of chronic ocular hypertension. Exp Eye Res, 2004. **79**(1): p. 75-83.

94. Grozdanic, S.D., et al., Functional characterization of retina and optic nerve after acute ocular ischemia in rats. Invest Ophthalmol Vis Sci, 2003. **44**(6): p. 2597-605.

95. Hood, D.C., et al., Blood vessel contributions to retinal nerve fiber layer thickness profiles measured with optical coherence tomography. J Glaucoma, 2008. **17**(7): p. 519-28.

AKNOWLEDGEMENTS

I am very happy to thank those who helped me in conducting this research, data analysis, and provided useful suggestions during the writing of this thesis.

First and foremost, I would like to thank my committee members; Drs. Steve Carlson, Donald Sakaguchi, and most especially, my major professor, Dr. Sinisa Grozdanic. You lifted me during a very volatile moment in my life and your kindness, care, concern, confidence, and intelligence strengthened my personality, and helped me gain independence. Many thanks to you!

I wish to thank all the members of our laboratory for their support and help in generating all data that is presented in this thesis. I am particularly grateful to Dr. Helga Kenova, who has been a great partner and adviser in many aspects of this work.

Special thanks to Drs. Tim Day and Michael Kimber for their support and encouragement.

Heartfelt thanks to my entire family for their constant encouragement and for providing me with a loving and caring environment.

I wish to thank my friends for their intelligent input, meaningful suggestions, and moral support throughout my tenure as a graduate student at Iowa State University.